A THz Pulse Radiator Based on PIN Diode Reverse Recovery

Sam Razavian and Aydin Babakhani

Department of Electrical and Computer Engineering
University of California, Los Angeles, CA 90095, USA
Samrazavian24@ucla.edu, Aydinbabakhani@ucla.edu

***Abstract*— This paper presents a fully integrated oscillator-less THz pulse radiator based on reverse recovery of a PIN diode implemented using 130-nm SiGe BiCMOS technology. The chip radiates a wideband frequency comb in the THz regime through an on-chip antenna. The spacing between the THz tones can be programmed up to 10.5 GHz by tuning the frequency of the input trigger. The spectrum of the radiated frequency comb is measured from 320 GHz to 1.1 THz with 5.5-GHz spacing between the tones. The Non-Linear Q-Switching Impedance (NLQSI) technique is used for tuning the frequency tones and increasing the stability of the output stage. At a distance of 4 cm from the pulse radiator, the measured SNRs (including the losses) with 1 Hz resolution bandwidth are 51, 40, and 21 dB at 0.6, 0.8, and 1 THz, respectively with a 10-dB line-width of less than 2 Hz. With a 5.5-GHz input trigger, the total power consumption of the chip is 45 mW, with 20 mW consumed by the driver stage.**

***Keywords*— BiCMOS, frequency comb, NLQSI, on-chip antenna, PIN diode, pulse radiator, reverse recovery, THz.**

I. Introduction

In recent years, broadband pulse generation techniques have been of great interest in the terahertz (THz) and mm-wave research due to wide range of applications, such as high-speed communication, high-resolution radars, spectroscopy, and remote sensing. Although different approaches and techniques have been proposed for THz wave generation, increasing the bandwidth and radiation power in THz systems remains challenging due to the limitations of silicon-based technologies. Most of recent the works in broadband pulse generation are based on the fast switching speed of transistors. In [1], by switching a bipolar transistor in a very short interval, pulses with full width at half maximum (FWHM) of 1.9 ps were achieved. Wideband frequency comb generation is also possible by switching a THz continuous wave (CW) radiator [2]; however, the bandwidth of the generated frequency comb is limited by the switching speed of the transistors. Dynamic pulse generation by controlling the phase and amplitude of the harmonic frequencies was proposed in [3]. Nevertheless, pulse generation using this approach is challenging, as programming the phase and amplitude of tones at mm-wave/THz frequencies requires complex circuit blocks.

Step-Recovery-Diodes (SRD) are popular for harmonic generation and frequency multipliers due to their ultra-sharp reverse recovery. However, SRDs are not available in silicon processes. As elaborated in the following sections, PIN diodes exhibit similar reverse recovery behavior to SRDs, which enables efficient harmonic generation.

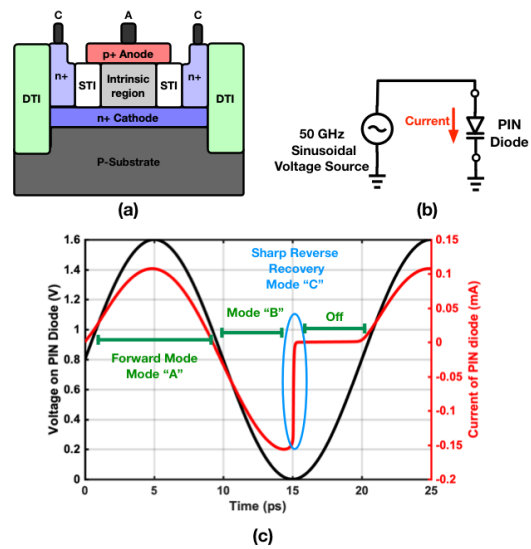

Fig. 1. (a) Structure of a PIN diode device in the SiGe 130-nm BiCMOS process, (b) Simple test-circuit to illustrate the sharp reverse recovery of a PIN diode, (c) Voltage and current waveforms of a PIN diode in different regions of operation.

In this work, the reverse-recovery of a standard PIN diode device in 130-nm BiCMOS technology is used to generate THz-pulses (wideband frequency comb), which are radiated through a broadband on-chip antenna. To the best of the authors' knowledge, this is the first PIN diode-based THz pulse radiator implemented in a silicon-based process.

II. Design Procedure

The structure of a PIN diode in 130-nm SiGe BiCMOS process is shown in Fig. 1. The detailed analysis of the reverse recovery of PIN diode is elaborated in [4]; however, to illustrate the sharp reverse recovery of a PIN diode, we consider the special case in which an ideal 50-GHz sinusoidal voltage source is applied across a PIN diode. To analyze the nonlinear behavior of a PIN diode, its operation can be divided into three separate intervals, as shown in Fig. 1. In mode "A," the diode is in forward mode, and holes and electrons are injected from N and P regions into the I-region. The amount of stored charge in the I-region depends on the carrier lifetime (τ) and amount of forward current. As the voltage across the diode drops, the current starts flowing in the reverse direction (region "B"), thus, depleting the excess charge stored in the I-region. When the I-region is fully depleted (mode "C"), the reverse current drops to zero with a time-constant determined by series cathode resistance (R_{CX}), off-state capacitance, and

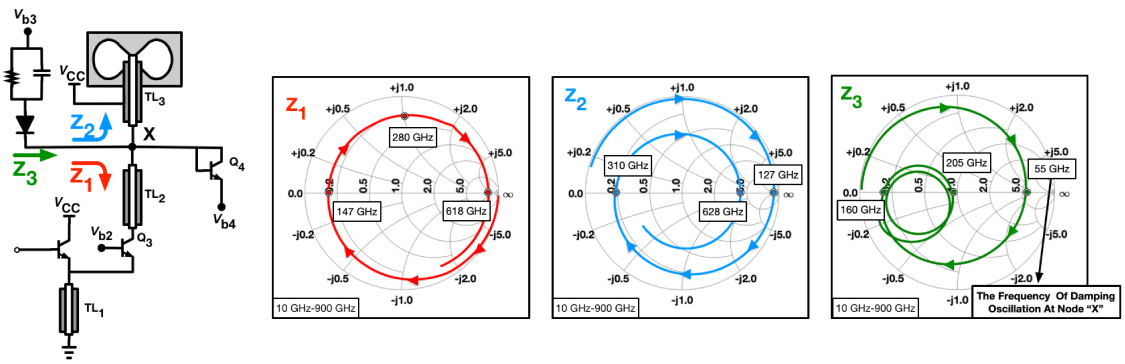

Fig. 2. Smith chart of the impedances at node X for broadband matching analysis.

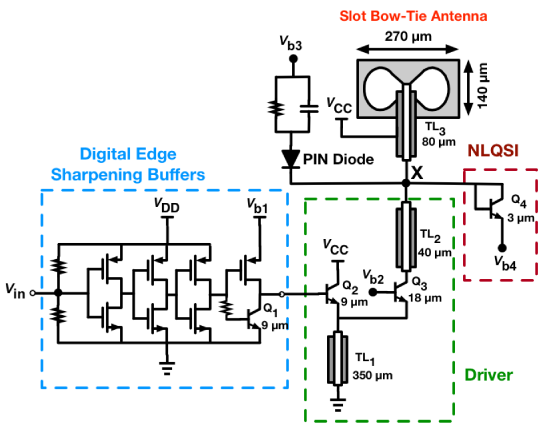

Fig. 3. Circuit schematic of the frequency-comb radiator.

the impedance of the circuit driving the PIN diode. Therefore, choosing the optimum size of the PIN diode is essential to achieve the shortest time constant. The sharp change in the current can generate THz tones at the load if proper matching is used. Note that the PIN diode should be driven with a large voltage swing in a certain frequency range in order to have a fast reverse recovery. For the driving signal at frequencies below 10 GHz, the amount of reverse current is not large enough to generate high-power THz tones. On the other hand, at high frequencies (above 100 GHz), the I-region cannot be fully depleted in each period; thus, the diode does not enter the highly nonlinear reverse region. Therefore, driving the PIN diode at the proper frequency is critical for pulse generation. Fig. 3 shows the architecture of the proposed broadband THz pulse radiator. The operation of each block is elaborated in the following sections.

A. Driver

To push the PIN diode to the highly-nonlinear region, a custom driver stage is designed (Fig. 3) that mimics the role of the 50-GHz source described in the previous section. The driver stage is switched by a series of edge-sharpening inverting buffers that are functional at frequencies as high as 10.5 GHz. Depending on the voltage level at the output of the digital buffers, the operation of the driver can be investigated in two separate intervals. When the output of the digital buffers is high, the driver stage is turned on. During this interval, the current flowing through the $TL1$ rises and the stored energy in $TL1$ increases. The amount of the current flowing through $TL1$ can be adjusted by tuning V_{b1}. In the second interval, driver (Q_2) is switched off abruptly via the inverting buffer (Q_1). In order to lower the transition time of the switching, an NPN BJT is used instead of an NMOS transistor in the last stage of the inverting buffers. Due to the abrupt switching of $Q2$, $Q3$ is turned on and the current flows through it. Consequently, a large ringing is generated at node X, which causes the PIN diode to operate in a highly-nonlinear region, as explained in the previous section. Proper wideband matching is essential in order to radiate the generated broadband pulses efficiently. To have a better understanding of the driver performance, the impedance at node X must be carefully analyzed (Fig. 2). Note that the effects of parasitics are included in our analysis with the aid of EM simulations and PDK models. The length and width of the $TL2$ are optimized so that the impedance seen from node X toward $TL2$ (Z_1) is sufficiently larger than the impedance seen toward $TL3$ (Z_3) over the frequency band of the radiation (Fig. 2). At the frequency of the damping oscillation at node X, $TL2$ can be neglected due to its short length. Without $TL2$, most of the generated THz power would be absorbed by the parasitic capacitors of Q_3 . Moreover, the length of the $TL3$ is tuned for a flat frequency-comb radiation over a wide band. It is worth mentioning that the total impedance seen at node X shows a strong resonance around $55\ GHz$, which is the frequency of the damping oscillation that drives the PIN diode into the nonlinear region.

B. Non-linear Q Switching Impedance

The abrupt switching of $Q2$ causes a large damping oscillation at node X. It should be noted that the frequency of the damping oscillation depends on poles and zeroes associated with node X rather than the frequency of the input trigger. As a result, the PIN diode enters the sharp reverse recovery region more than once in a period due to the oscillation at node X; therefore, unsynchronized pulses are generated. This effect causes undesired nulls and peaks in the frequency spectrum of the radiated signal. The NLQSI

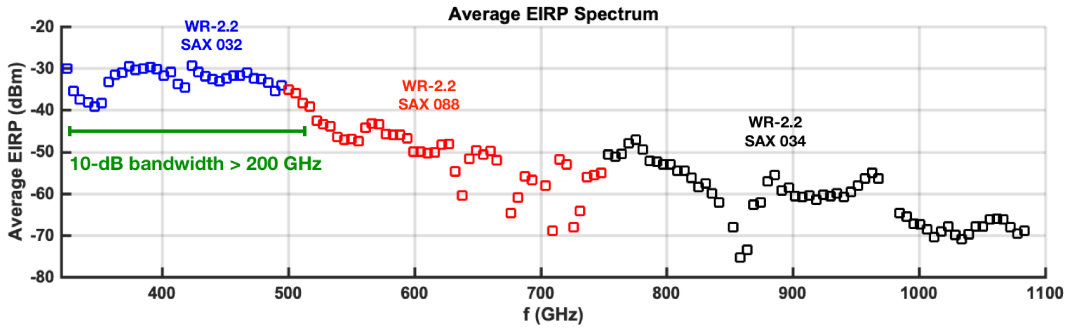

Fig. 4. Calculated average EIRP based on the measurement results.

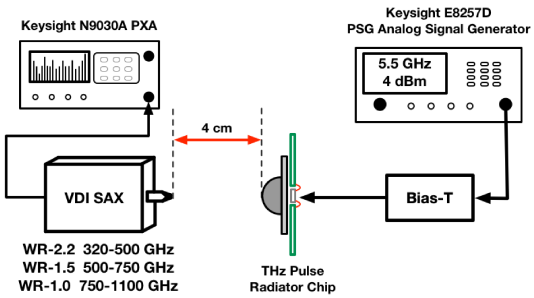

Fig. 5. Setup for the measurement of the EIRP.

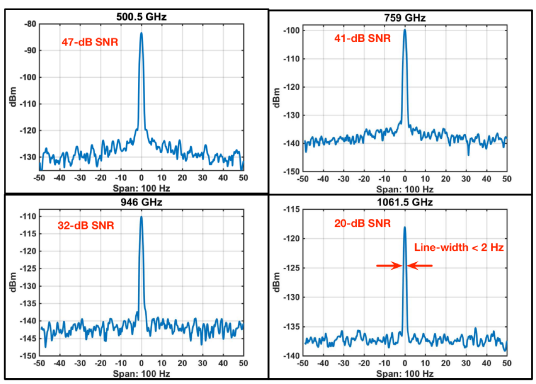

Fig. 6. Measured THz tones of the radiated frequency comb.

approach is utilized to prevent nulls and peaks in the frequency spectrum [5]. $Q4$ begins conduction, when voltage at node X reaches a certain threshold. Consequently, the Q-factor is reduced, and the oscillation is damped at a faster rate. As a result, the PIN diode is pushed into the sharp reverse recovery region (highly nonlinear region) once in a period. Moreover, due to large current switching at the driver stage, the circuit is prone to undamped oscillation. Q_4 guarantees that the circuit remains stable by decreasing the Q-factor in the case of an oscillation.

C. Broadband On-Chip Antenna

At mm-wave/THz frequencies, off-chip antennas are not suitable due to the long, lossy, inductive interconnects (wire-bonds, PCB traces, etc.). One the other hand, on-chip antennas can be integrated in proximity to the other blocks of the circuits, thus benefiting from a larger bandwidth and higher efficiency. For broadband radiation, a custom-designed coplanar waveguide-fed (CPW) slot bow-tie antenna is used. For simulation purposes, the input impedance of the antenna is simulated over the desired frequency range and modeled using lumped components for circuit simulations.

Radiation efficiency of on-chip antennas is poor in the bulk processes, since a large portion of the radiation gets trapped in the lossy silicon substrate (in the form of substrate modes). To tackle this problem, a hemispherical, high-impedance silicon lens is placed under the chip, which substantially improves the bandwidth and radiation efficiency of the antenna by eliminating the substrate modes.

III. Chip Characterization

Fig. 5 shows the setup for chip characterization in the frequency domain. Based on the dimensions of the antenna and the silicon lens, to ensure a far-field mode of radiation, the receiver antenna is placed at a 4-cm distance from the chip for frequencies above 320 GHz. Virginia Diodes spectrum analyzer extenders (VDI SAX) for three separate bands are used for obtaining the spectrum of the received signal from 320 GHz up to 1.1 THz. The average effective isotropic-radiated power (EIRP) in Fig. 4 is calculated for each frequency point based on the Friis transmission formula and the EM simulation of antenna. For EIRP calculations, the loss of the cables, antenna loss, VDI SAX IF amplification, and mixer conversion loss (using the VDI SAX calibration test data for each frequency point) are calibrated. As observed in Fig. 4, there are some sharp fluctuations in several regions of the spectrum, which stem from different factors, including nulls due to the silicon lens, EIRP measurement error, and VDI SAX calibration test data error for each band. In addition, the raw tones (embedded loss) on the spectrum analyzer are shown in Fig. 6.

Due to the limited bandwidth of the electronic oscilloscopes, the time-domain measurement of the radiated waveform is challenging. On the other hand, optical THz-TDS systems, provide a large bandwidth for capturing the wideband waveforms. In order to perform time-domain measurement, we have designed a setup (Fig. 7) utilizing an Advantest TAS7500TS femtosecond-laser-based THz sampling system. Note that the input trigger of the chip must be locked to

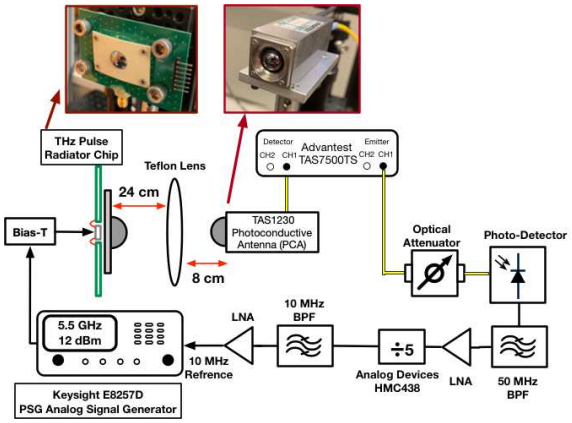

Fig. 7. Time-domain measurement setup

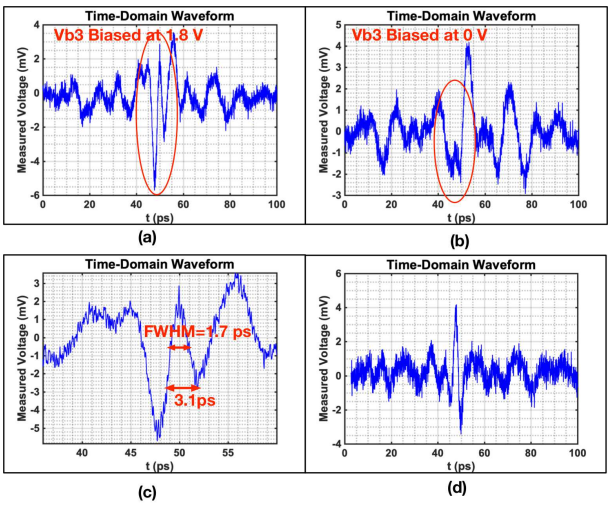

Fig. 8. Time-domain waveforms of the radiated pulse. a) The PIN diode is biased at 1.8 V. b) PIN diode is biased off. c) Zoomed version of (a). d) Subtraction of (b) and (a).

the THz-TDS system; otherwise, due to the frequency drift of the input trigger, the signal disappears during averaging due to significant jitters. To address this issue, the signal generator is locked to the THz-TDS system using the approach demonstrated in Fig. 7. The resultant time-domain waveform of the radiated pulse after an averaging number of 256 is shown in Fig. 8, which shows a FWHM of 1.7 ps.

IV. Conclusion

This paper reports a fully integrated on-chip THz pulse radiator based on reverse recovery of a PIN diode. The repetition rate of the generated pulses is programmable using the input trigger, which can be tuned to as high as 10.5 GHz. The power consumption of the driver stage is 20 mW at 5.5 GHz repetition-rate. An on-chip slot bow-tie antenna is employed for radiating the THz pulses with the a total efficiency above 60% over the band of radiation. The spectrum of the radiated pulses was measured from 320 GHz up to 1.1 THz using the VDI SAX and the Keysight N9030A PXA signal analyzer. Table 1 shows the comparison between this work and similar prior works. Based on Fig. 4, this work demonstrates higher radiation power at frequencies above 300 GHz, a flatter average ERIP spectrum, and lower power consumption compared to the state of the art. A micrograph of the fabricated chip is shown in Fig. 9.

Table 1. Comparison With Prior Works

Performance	This work	[1]	[6]	[3]
Highest frequency measured	1.1 THz	1.1 THz	110 GHz	214 GHz
Pulse width (FWHM)	1.7 ps	1.9 ps	26 ps	2.6 ps‡
Repetition rate	50 MHz to 10.5 GHz	50 MHz to 5.5 GHz	1.364 GHz to 1.519 GHz	N/A
Pulse generation technique	D2I†	D2I*	Oscillator-based	Oscillator-based
Die Area (mm^2)	0.48	0.47	6.16	2.5
Power consumption	20 mW	105 mW	1400 mW	N/A
Technology	130-nm SiGe BiCMOS	130-nm SiGe BiCMOS	130-nm SiGe BiCMOS	65-nm CMOS

†Digital-to-Impulse architecture based on PIN diode reverse recovery
*Digital-to-Impulse architecture based on switching of a BJT
‡ Simulated result

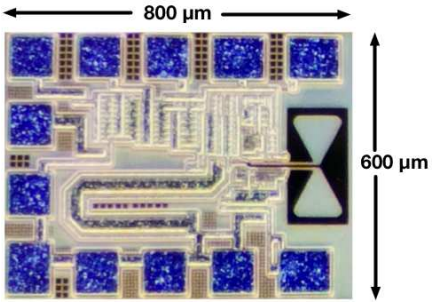

Fig. 9. THz pulse radiator die photograph

Acknowledgment

The authors thank the National Science Foundation Career Award program for supporting this work.

References

[1] M. M. Assefzadeh and A. Babakhani, "Broadband oscillator-free thz pulse generation and radiation based on direct digital-to-impulse architecture," *IEEE J.Solid-State Circuits*, vol. 52, no. 11, pp. 2905–2919, Nov. 2017.

[2] R. Han and E. Afshari, "A 260ghz broadband source with 1.1mw continuous-wave radiated power and eirp of 15.7dbm in 65nm cmos," *IEEE International Solid-State Circuits Conference Digest of Technical Papers*, pp. 138–139, 2013.

[3] X. Wu and K. Sengupta, "Dynamic waveform shaping for reconfigurable radiated periodic signal generation with picosecond time-widths," *2015 IEEE Custom Integrated Circuits Conference (CICC)*, pp. 1–4, 2015.

[4] S. Schunemann and J. Muller, "A charge-control model of the pin diode," *IEEE Trans. Electron Devices*, vol. 23, no. 10, pp. 1150–1158, Oct. 1976.

[5] P. Chen, M. M. Assefzadeh, and A. Babakhani, "A nonlinear q-switching impedance technique for picosecond pulse radiation in silicon," *IEEE Trans. Microw. Theory Techn*, vol. 64, no. 12, pp. 4685–4700, Dec. 2016.

[6] A. Arbabian, S. Callender, S. Kang, M. Rangwala, and A. M. Niknejad, "A 94 ghz mm-wave-to-baseband pulsed-radar transceiver with applications in imaging and gesture recognition," *IEEE J.Solid-State Circuits*, vol. 48, no. 4, pp. 1055–1071, Apr. 2013.